Summary report

On

"Development of nanocarrier based thermosensitive mucoadhesive gel containing Metformin Hydrochloride and Silymarin for Treatment of Oral Cancer"

To be submitted

to

Research & Recognition Committee Meeting

Of

Ph. D

Programme In

Pharmaceutical Sciences

By

Meghanath B. Shete

Supervisor

Dr. Ashwini S. Deshpande
Professor & Associate Dean
SPTM, Hyderabad

Date of Registration: 21 July 2018

Shobhaben Pratapbhai Patel

School of Pharmacy and Technology Management

SVKM's Narsee Monjee Institute of Management Studies

V.L. Mehta Road, Vile Parle (W), Mumbai-400056

Index

Sr. No.	Contents	Page no.
1	Objectives	3
2	Introduction	4
3	Experimental methodology	6
4	Results and discussion	10
5	Publications, conferences, Grants, and workshops	33
6	References	34

Objective

Development of Nanocarrier based Thermosensitive Mucoadhesive Gel containing Metformin-Hydrochloride and Silymarin for Treatment of Oral Cancer.

Supporting objectives

1) To formulate and characterize suitable nanocarrier system
2) To develop thermosensitive gel incorporated with nanocarrier system
3) To perform *in-vitro*, *ex-vivo* and *in-vivo* evaluations

Introduction

Oral cancer (OC) is a commonly known subtype of head and neck cancer. It is currently ranked 16th overall in malignant cancers due to a heavy worldwide burden. Almost 7,44,994 deaths were reported worldwide in 2020. Of those, 5,73,775 deaths among males and 1,71,219 deaths among women were reported, respectively (1). The squamous epithelial cells of the oral cavity contribute to over 90% of malignancies with an overall survival rate of 40-50 % (2). At present, three gold-standard treatment options including surgery, radiotherapy, and chemotherapy have been used for OC treatment. These treatment strategies are associated with some limitations like the removal of several functional and aesthetic organs (3), DNA damage, and increased risk of colon, liver, and lung cancers. the systemic application of chemotherapeutic bioactive often gives dose-related toxicity, drug resistance, and off-targeting effect. However, there is currently no drug delivery system available for the controlled administration of anticancer bioactive to the oral cavity (4).

The mouth cavity offers the availability of external surfaces, non-invasive and easy topical self-application, and removal of dosage forms. The goal of the mucoadhesive topical deliveries for oral cancer is to interact with the mucosa to attach and to precise delivery drugs to local tumor site by accumulating in it.

Silymarin is one of the key active compounds derived from the seeds of the plant *Silybum marianum.* It exhibits multiple biological actions such as hepatoprotective, antioxidant, anti-inflammatory, anticarcinogenic, and pro-apoptosis, and is also given as a dietary supplement, etc. Extensive research demonstrated that SME is used as an anticancer agent for a wide variety of cancers including OC. In this research work the we have selected second drug Metformin Hydrochloride the different activities of MET against cancer such as anti-proliferative effects, antiangiogenic effects, and antitumor actions (5-9). Lately, antitumor studies revealed that MET offers the potential to increase ROS in cancerous cells to promote cell death (10). A mixture of

solid and liquid lipids stabilized by surfactants produce a submicron structure known as NLCs. *In-situ* gel (ISG) forming systems are fluids at room temperature and converted into the gel in response to several external stimuli, such as temperature, pH, and solvents (11). These systems are free-flowing at room temperature but solidify after application into the body.

Part-1: Methodology for Enhancement of in-vitro anti-oral cancer activities of silymarin using dispersion of nanostructured lipid carriers in mucoadhesive in-situ gel

In this research work, before formulation of NLCs, we performed preformulation studies for SME including physical identification, melting point determination, XRD, DSC analysis, drug-excipient compatibility studies by FTIR. In addition, we developed the UV spectroscopical method for estimation of SME from formulation. In the formulation part, we screened the composition of NLCs to encapsulate the silymarin using previously reported solubility method (12). SME-NLCs were formulated using the melt-emulsification method after that subjected to the probe sonication (13). For selecting the influence of formulation variables and process variables on formulation parameters, Taguchi Orthogonal Array (TOA) design was employed with 7 factors and 8 run experiments.

Further, Response surface methodology (RSM) was employed to quantify the relationship between independent variables like the solid lipids: liquid lipid (A), the concentration of surfactant (B), and probe sonication time (C) with dependent variables such as PS (X), PDI (Y), and % EE (Z) as shown in Table 1. A Design-Expert Stat-Ease, Trial version 11, Inc., Minneapolis, USA software used for the optimization of NLCs formulation with minimum experimental batches. The BBD with 3-variable and 3-level (3^3) with three center points have resulted in a set of 15 experimental batches. The best-fit quadratic polynomial equation was mentioned as equation 1

$$Y= b_0+b_1A+b_2B+b_3C+b_{12}AB+b_{13}AC+b_{23}BC+b_{11}A^2+ b_{22}B^2+b_{33}C^2 \qquad (1)$$

Where Y represents the independent variable, b_0 indicates the intercept, b_1 to b_{33} represents the regression coefficient calculated from the observations of individual responses, and A, B, and C represent the independent variables.

Table 1 Independent variables used in RSM-BBD of SME-NLCs

	Levels		
Independent variables	**+1**	**0**	**-1**
Ratio Solid lipid: liquid lipid (A)	70	60	50
Concentration of surfactant (%) (B)	1.5	1.25	1
Sonication time (min) (C)	20	15	10

The developed SME-NLCs were further characterized for the PS, PDI, %EE, %DL, FTIR, DSC, PXRD studies. Morphological features of developed SME-NLCs were characterized by the SEM studies. *In-vitro* release behavior of SME from Compritol-based nanostructured lipid carriers was estimated (14) using a dialysis membrane (12-14 kDa molecular weight cut off, Himedia, Mumbai). The release of SME from NLC compared with the 1 % w/v SME solution prepared with 40% ethanol. In addition, the developed nanoformulation was subjected to the at 30±2°C/65%±5% RH for 90 days and checked regularly for any variations in the physicochemical parameters like PS, PDI, and EE (%) and compared with initial zero-month data (15).

We prepared a mucoadhesive *In-situ* gel system containing SME-NLCs using reported (16). In this work, variable amount of Plx and CP were used to select the optimum quantity of both that shows gelling at 37 °C (17). The developed gel formulation was further studied for gelling time, gelling temperature, viscosity measurement, *ex-vivo* permeation studies, *ex-vivo* mucoadhesion, and cell line studies.

In the further studies, the performance of the developed SME-loaded NLCs incorporated in the mucoadhesive gel system were examined for *in-vitro* cytotoxicity studies, ROS levels, cell cycle studies and internalization studies on the cancerous KB cells.

Part-2: Methodology for Nanostructured lipid carrier loaded-metformin hydrochloride: Design, optimization, characterization, assessment of cytotoxicity and ROS evaluation

The main objective of this research work was to develop the NLC carrier system to encapsulate the water-soluble drug and to determine the effect of plain drug and MET loaded NLC on oral cancer KB cells. We performed the preformulation studies such as identification of MET, crystallinity and thermal behavior of MET using XRD and DSC techniques respectively. Maximum wavelength was determined using spectrophotometer in water.

To develop NLCs, composition of formulation was screened using MET solubility in the several lipids. A reported method was used to prepare $_{GMS}$MET-NLCs (18). A Three factor-three level (3^3) Box Behnken design was used to evaluate the NLC composition on the physicochemical properties using Design Expert software 11 (State-Ease Inc., USA). Based on the preliminary trials, lipid ratio (A), surfactant concentration (B), and sonication time (C) were selected as independent variables. Here, their impact was interpreted at three levels coded as -1, 0, +1 on dependent variables viz. PS (Y1), PDI (Y2)), and EE (%) (Y3). A computer-generated second-order polynomial quadratic equation is shown as equation (1),

$Y = \alpha_0 + \alpha_1\beta_1 + \alpha_2\beta_2 + \alpha_3\beta_3 + \alpha_{12}\beta_1\beta_2 + \alpha_{13}\beta_1\beta_3 + \alpha_{23}\beta_2\beta_3 + \alpha_{11}\beta_1^2 + \alpha_{22}\beta_2^2 + \alpha_{33}\beta_3^2$ ..... (1)

Where, individual responses, intercept, and regression coefficients of individual and interactive terms of independent factors A, B, and C are indicated by Y, α0, and β_1 to β_{33}, respectively. While independent variables are Y_1, Y_2, and Y_3 as chosen responses, as shown in Table 1.

Table 1 shows the variables and their levels in the optimization of $_{GMS}$MET-NLCs

	Independent variables		
Levels	**A: Ratio of solid lipid to liquid lipid (%)**	**B: Concentration of surfactant (%)**	**C: Sonication time (min)**
-1	50	0.5	5
0	0	1	7.5
+1	90	1.5	10
	Dependent variables		
	Y_1: PS (nm)	Y_2: PDI	Y_3: EE (%)
Goal	CpK	CpK	CpK

The developed $_{GMS}$MET-NLCs were analysed for particle size, PDI, ZP, EE, DL. In addition FTIR, DSC, PXRD and SEM studies were performed (19, 20). Further, the *in-vitro* release of MET was analyzed in simulated saliva fluid and analyzed the release kinetics (21). The optimized formulation was subjected to the storage stability studies at 25 ± 2°C/60 ± 5 RH, and 40 ± 2°C/75 ± 5 RH for 3 months. In the biological evaluations, cell viability and ROS studies were performed against KB oral cancer cells.

Part 3: Preparation and *in-vitro* evaluation of lipid nanostructures integrated buccal mucoadhesive thermosensitive gel for dual delivery of silymarin and metformin

In this research wok, we aimed to encapsulate both silymarin (SMR) and metformin (MTR) in NLCs. In other works, we have encapsulated individual drugs in in NLCs and examined on oral cancer cells. It is worthy to mention her that we are the first to encapsulate these two drugs in examine the anticancer effect on the oral cancer cells.

Herein, we have used the previously used method for preparation of NLCs. Both the drugs were encapsulated in 1:1 ratio. In this research work, we examined the compatibility between silymarin and metformin hydrochloride. Based on the reported literature, we selected the Compritol and oleic acid for preparation of NLCs. Kolliphore P188, Tween 80, Tween 20, and Kolliphore RH 40 were employed to select the appropriate surfactant based on the PS, PDI, and ZP of prepared NLC by using individual surfactant. Further to optimize the lipid ratio we have performed the trial formulation batches of SME/MET-NLC with different ratio of solid as to lipid at 50:50, 60:40 70:30, 80:20 and, 90:10. And checked for separation of oil from mixture.

The developed dual drug loaded NLCs were evaluated for the PS, PDI, ZP, and EE. The morphology of the developed NLC was analysed using SEM, TEM and AFM (22) studies. *In-vitro* release was conducted for SME and MET from the NLCs in SSF pH 6.8. Further, these developed NLCs were incorporated in the mucoadhesive gel system prepared by using combination of poloxamer 407 (18% w/v) and gellan gum (0.5 % w/v).

The prepared SMR/MTH-NLCs-gel was evaluated for the gelling-temperature (23), viscosity, mucoadhesive streghth (24) and *ex-vivo* release study (using goat buccal mucosa). In addition, the prepared formulation was analyzed for the cell viability studies against KB oral cancer cells.

Results and discussion

Part-1: Methodology for Enhancement of in-vitro anti-oral cancer activities of silymarin using dispersion of nanostructured lipid carriers in mucoadhesive in-situ gel

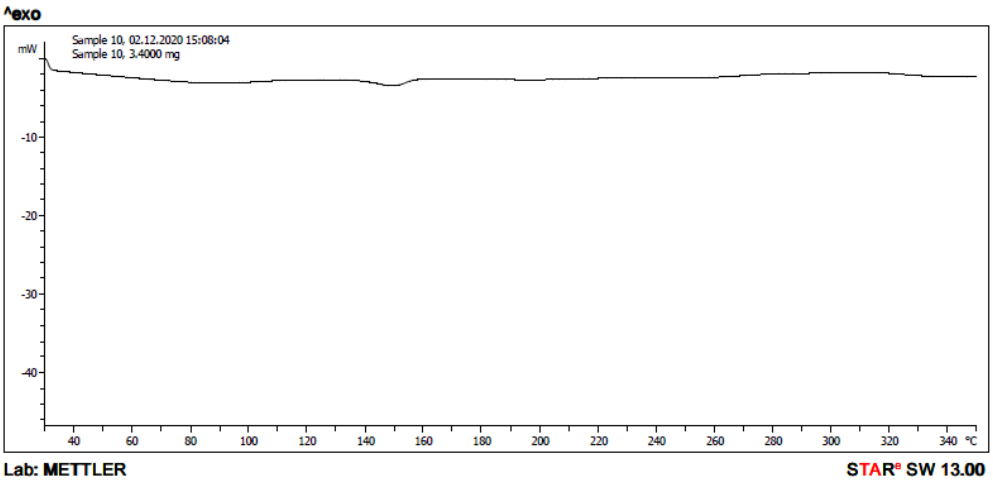

Fig. 1 represents the DSC thermogram of Silymarin

In the preformulation studies, the physical properties of SME found satisfactory as per the reported literature. Fig. 1 shows the DSC thermogram at 147 °C. In compatibility studies, SME demonstrated the compatibility between formulation excipients for 1 month. (FTIR spectra are not shown here) In the composition screening studies, Compritol, Miglyol and Tween 80 showed the maximum solubility compared with the other lipids and surfactant. Table 2(a) and (b) showed the results of solubility studies.

Table 2 (a) Shows the solubility of SME (Mean ± SD, n=3)

Sr. No.	Lipids	Solubility (mg/mL)
1	Oleic acid	0.52 ± 0.03
2	Capryol 90	0.17 ± 0.10
3	Miglyol 812 N	0.96 ± 0.07
4	Olive oil	0.87 ± 0.05
	Surfactants	
5	Tween 80	0.36 ± 0.10

6	Tween 60	0.01 ± 0.03
7	Tween 20	0.17 ± 0.09
8	Colliphore RH 40	0.27 ± 0.06

Table 2 (b) Representing SME solubility in (Mean values, n=3)

Sr. No.	Solid lipids	Number of parts of solid lipid required to dissolve unit part of SME
1	Compritol 888 ATO	10 parts
2	Precirol ATO 5	12.5 parts
3	Cetyl palmitate	15 parts
4	Kolliwax GMS II	17 parts
5	Dynasan 116	20.5 parts

In the Taguchi orthogonal array studies as shown in Fig. 2 we observed, the lipid and surfactant concentration, and probe-sonication time were found to have impact on the chosen formulation and process parameters. These factors were further optimized by using BBD. Fig. 3 illustrates the impact of the interactions of the selected variables on the chosen dependent variables were analysed using 3- D surface plots and statistically analyzed. Further, the optimized formula was achieved using the design space approach. The flagged values in the overlay plot were 59.02 %, 1.15 %, and 10 min for the ratio of solid lipid to liquid lipid, surfactant concentration, and probe sonication, respectively. The achieved formula by the software was validated by producing 3 batches and the average values of PS 315.5 ± 0.10 nm, PDI 0.341 ± 0.01, % EE 71.05 ± 0.05 %, ZP -14.01 ± 0.21 mV, and % DL 6.95 ± 0.20 %

The FTIR analysis (Fig. 4) confirms no significant interaction of SME with the formulation components was developed was found compatible with each other (25). The DSC studies shown in Fig. 5 for lyophilized SME-NLCs depicted that SME was incorporated in lipid matrix as the endothermic peaks of SME showed peaks with lowering of intensities (26). XRD studies (Fig. 6)

showed that Lyophilized SME-NLC formulation showed a considerable decline in the intensity of diffraction peaks because SME was completely dispersed in lipids of NLC. The smooth surfaces were confirmed from the SEM studies of optimized formulation (Fig 7). The nanoparticles were found to be spherical with more or less smooth surfaces. The spherical nanoparticles are attributed to good prolonged release of the drug and help to protect the incorporated natural compounds form the enzymatic degradation in the oral cavity (27). However, at random places, clumps of the particles were observed, which might be due to the probable shrinkage issues of NLCs or the lesser concentration of the dispersion medium during the drying process of the particles were observed, (as shown in Fig. 8), SME showed after 24 h only 72 % release with initial first- order followed by the slow diffusion from the lipids.

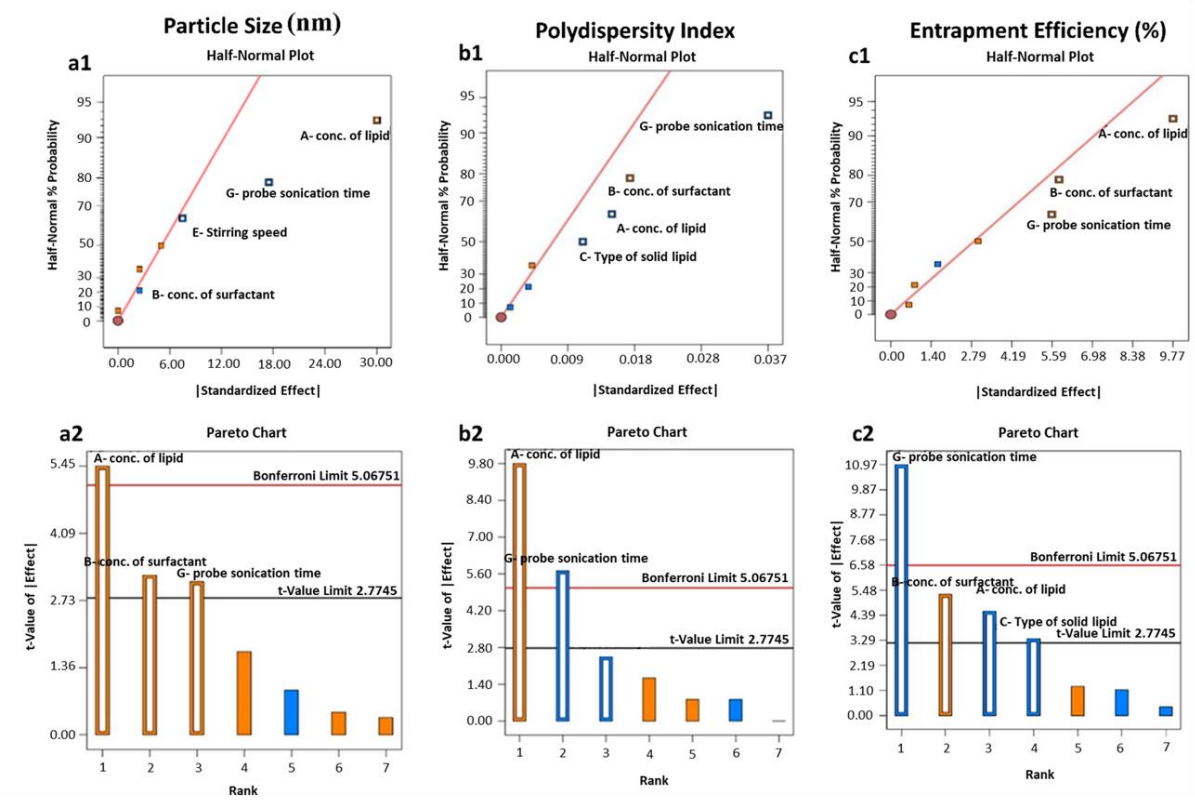

Fig. 2. a_1, b_1, and c_1 represent the half-normal plots, and a_2, b_2, and c_2 represent the Pareto charts for illustrating the effects of the chosen material and process variables on PS, PDI, and (%) EE obtained by Taguchi orthogonal design

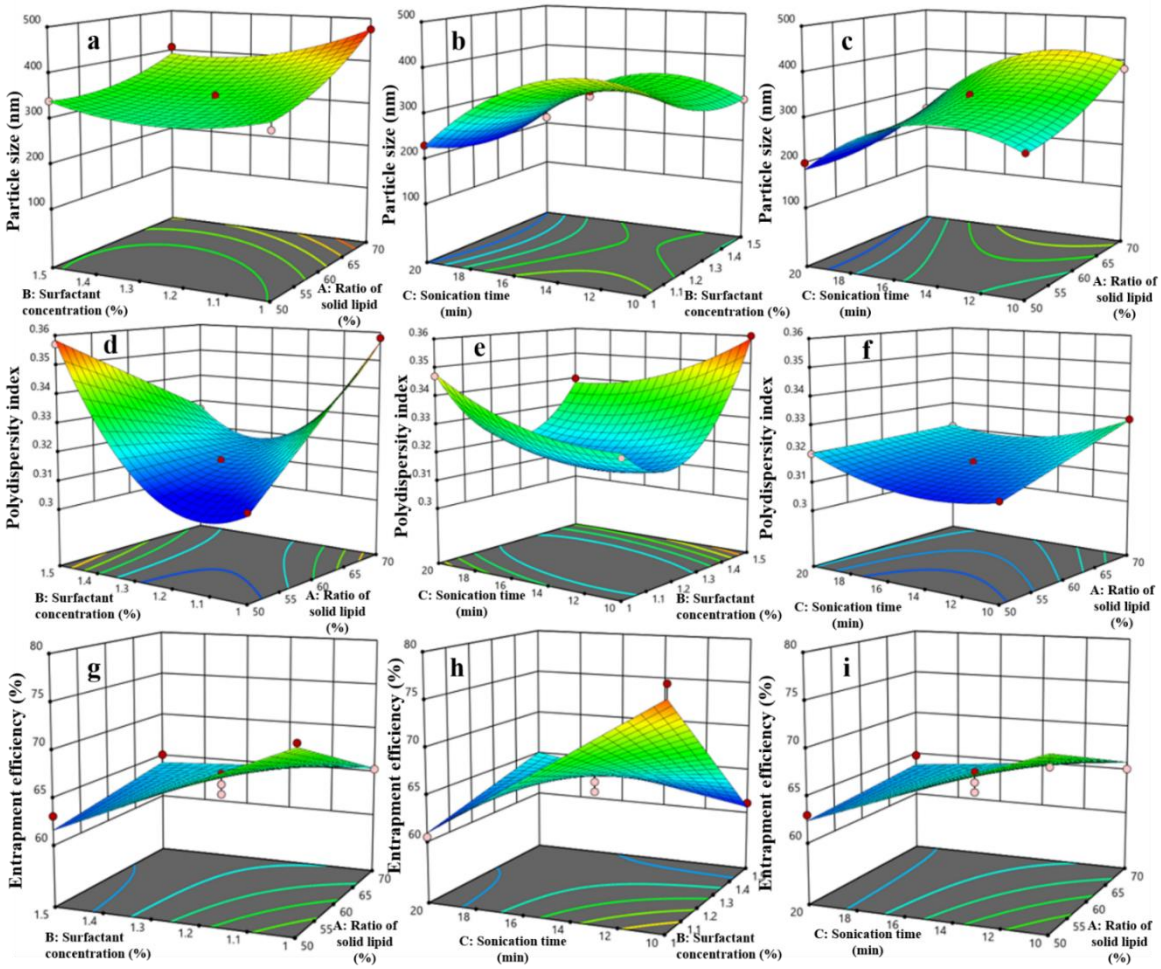

Fig. 3. 3-D curves to show the influence of independent variables to dependent variables such as PS (a-c), PDI (d-f), and % EE (g-i)

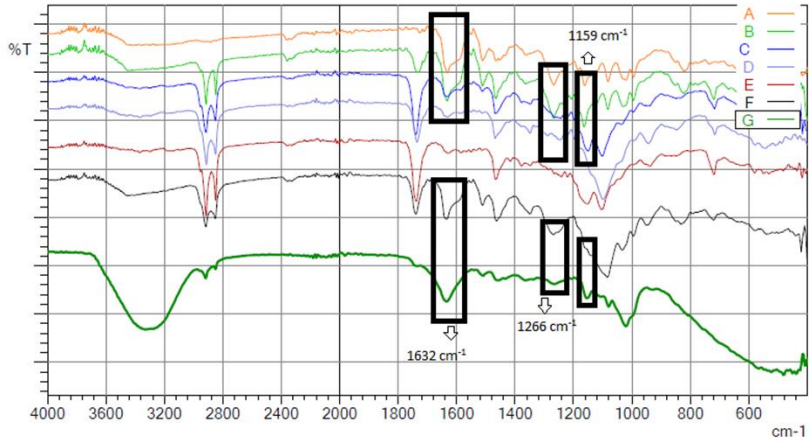

Fig. 4. IR spectra of (A) SME, (B) SME + Compritol 888, (C) SME + Miglyol 812 N, (D) SME +Tween 80, (E) Physical mixture of excipients without SME, (F) Physical mixture of

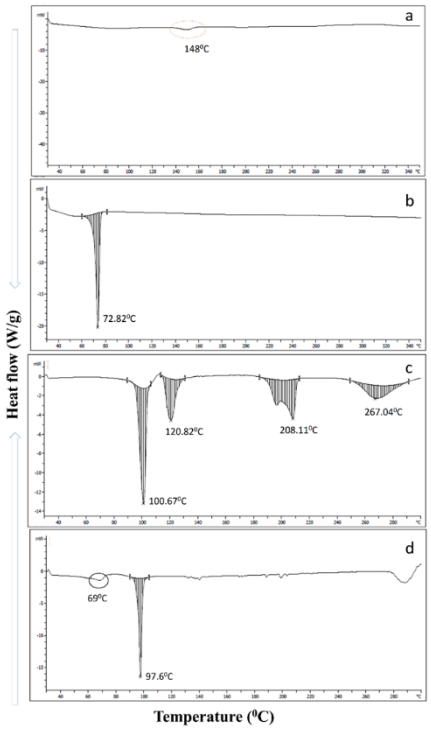

Fig. 5. Thermogram (a) Pure SME, (b) Compritol 888, (c) Trehalose, and (d) SME-NLC

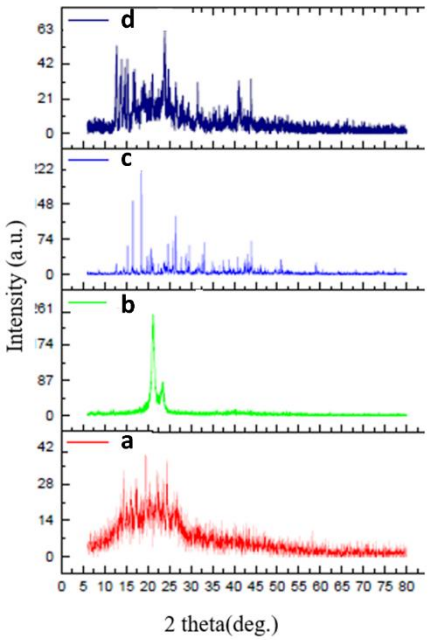

Fig. 6. XRD pattern of (a) Pure SME, (b) Compritol 888, (c) Trehalose, and (d) SME-NLC

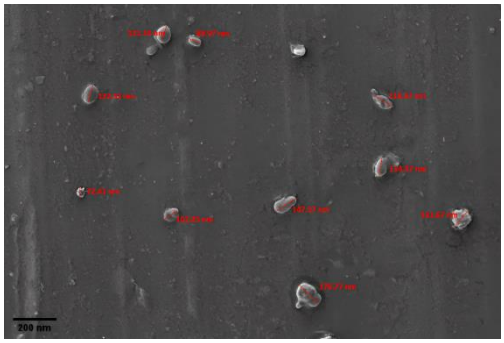

Fig. 7. Scanning electron microscope image of optimized SME-NLCs

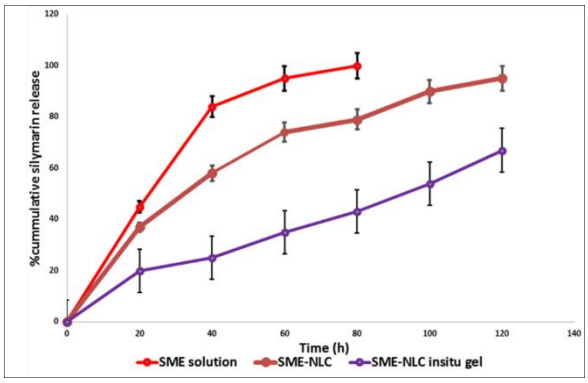

Fig. 8. *In-vitro* SME release profile from NLCs formulation and *ex-vivo* permeation

Further, combination of Plx (18 % w/v) and CP (0.5% w/v) were selected based on the results (28) demonstrated in the Table 3 (a) and (b).

Table 3 (a) Various concentrations of Poloxamer 407 for the study (Mean ± SD, n=3)

Sr. No.	Plx concentration (% w/v)	Gelation Temperature (^{0}C)	Gelation time (Sec)
1	16	43.0 ± 0.6	57 ± 0.2
2	17	32.7 ±0.2	43 ± 0.3
3	18	35.5 ± 0.1	35 ± 0.2
4	19	30.0 ± 0.1	31 ± 0.3
5	20	28.5 ± 0.2	27 ± 0.1

Table 3 (b) *In-situ* gel evaluation of different batches (Mean ± SD, n=3)

Gel formulations	Gelation temperature (°C)	Viscosity (cps)	Gel strength (s)	Mucoadhesive strength (dynes/cm^2)
AB1	33.2 ± 0.5	2789 ± 173	47 ± 2.1	4575 ± 200
AB2	31.6 ± 1.2	3342 ± 201	59 ± 0.2	6050 ± 208
AB3	29.3 ± 0.9	3501 ± 105	65 ±0.8	9780 ± 508

The mucoadhesive gel demonstrated ~21 % of the SME was released from the gel and can continue to release beyond 120 h (29). Fig. 9 shows the IC_{50} values for free SME and SME-NLCs were found to be 36.60 ± 0.26 µM and 28.40 ± 0.89 µM respectively. Interestingly, a much-reduced value i.e., 24.90 ± 0.45 µM was found for cells treated with SME-NLCs-Plx/CP-G. This may be due to the fast cellular uptake of NLCs plus the availability of SME-NLC to the KB cells.

ROS generation studies (Fig. 10) demonstrated the escalated level of ROS in KB cells for SME-NLCs and SME-NLCs-Plx/CP-ISG in comparison with plain SME, however, no significant difference in the control levels and SME-NLCs-Plx/CP-ISG. Fig. 11 depicts that an increase the percentage of SME-NLCs-Plx/CP-ISG in the Sub-G0 phase of cell cycle complemented by a progressive decrease in the G1, S, and G2/M phases which is indicative drug induced cell death (30). The internalization studies (Fig. 12) showed increased incubation time resulted in improved internalization of SME-NLCs into KB cells, indicated by the high intensity of the green fluorescence.

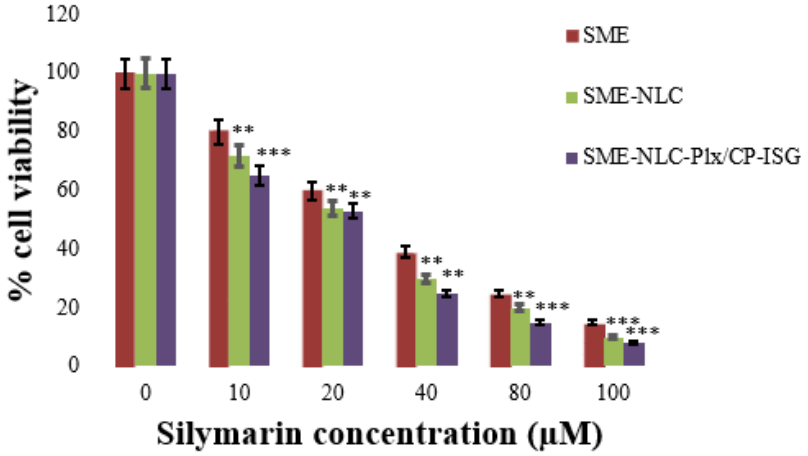

Fig. 9. % Cell viability of KB cells on the treatment of free SME, SME-NLC, and SME-NLC-Plx/CP-ISG. Results were represented as Mean ± SEM (n=3) *$p < 0.05$, ** $p < 0.005$, and *** $p < 0.0005$. The SME-NLC and SME-NLC-Plx/CP-ISG was compared statistically with SME using one way ANOVA followed by Dunnett's test at 95% confidence interval.

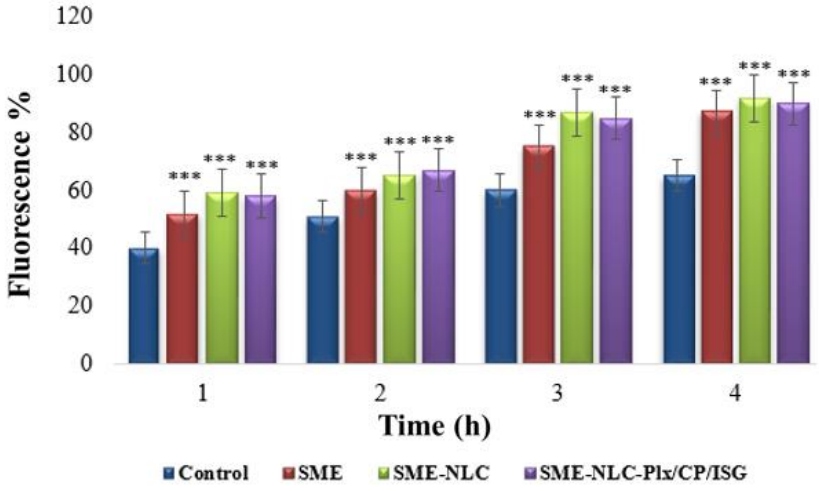

Fig.10. ROS study for control, free SME, SME–NLCs, and SME-NLC-Plx/CP-ISG. Cells without treatment considered as control. The SME-NLC and SME-NLC-Plx/CP-ISG was compared statistically with SME using one way ANOVA followed by Dunnett's test at 95% confidence interval where, $p < 0.05$ is considered as statistically significant

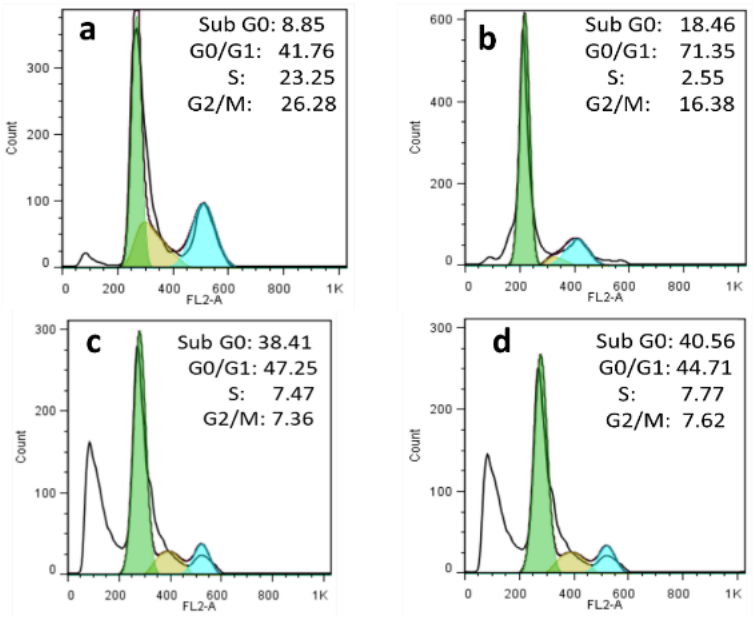

Fig. 11. Cell cycle analysis of (a) SME free NLC, (b) SME, (c) SME-loaded NLCs, and (d) SME-NLC-Plx/CP-ISG

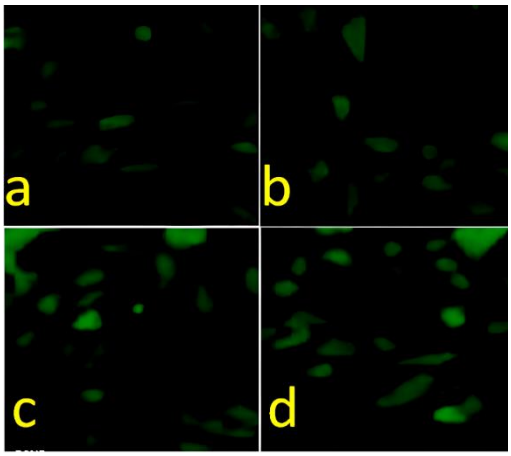

Fig. 12. Cellular uptake images of FITC-labelled SME-NLCs formulation by KB cells for 1 h to 4 h, Green fluorescence belongs to FITC

Results and Discussion

Part-2: Methodology for Nanostructured lipid carrier loaded-metformin hydrochloride: Design, optimization, characterization, assessment of cytotoxicity and ROS evaluation

The purity of MET was analyzed by FITR and determination of λmax using UV spectroscopy. The Fig. 13 showed that all the characteristic peaks (Table 4) are similar with reference standard and λmax found to be 232.7 nm (Fig. 14)

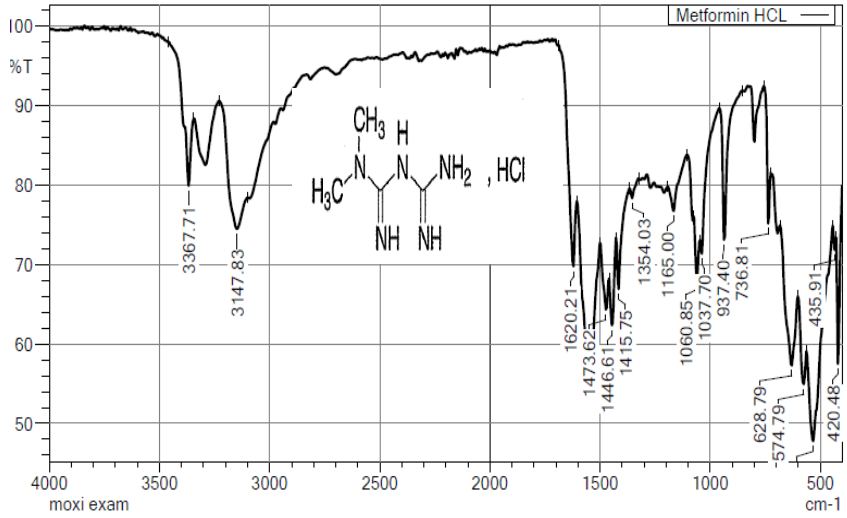

Fig. 13 FTIR spectra of Metformin hydrochloride

Table 4 Characteristic peaks of Metformin Hydrochloride

Sr. No.	Standard values(cm^1)	Obtained Values (cm^1)	Inference
1	1350-1050	1354-1165	C-N stretch
2	1580-1650	1620	N-H bending (in-plane)
3	3350-3450	3367,3350	N-H symmetric and asym. stretch of primary amine
4	~1100	1060	C-N stretch
5	~ 1600	1620	C=N stretch

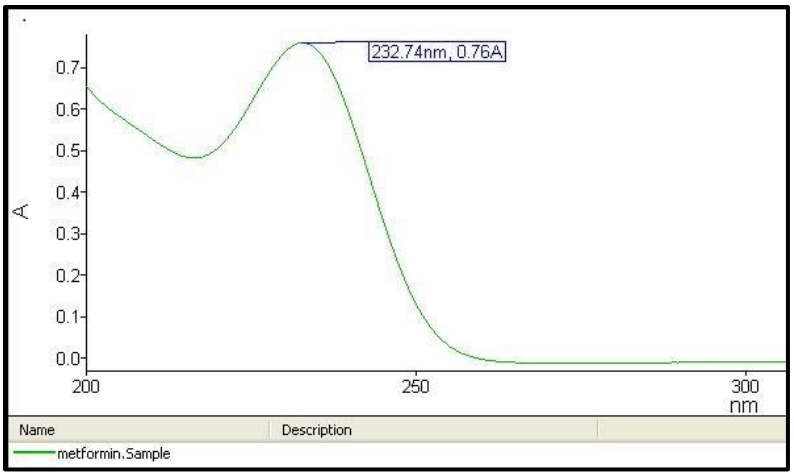

Fig. 14 shows λmax of metformin hydrochloride

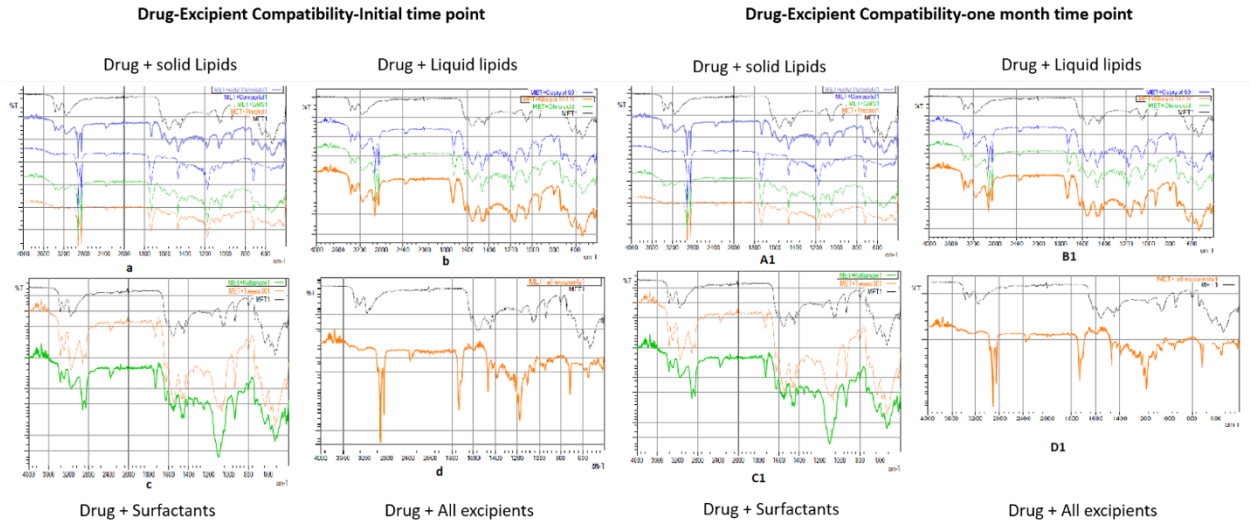

Fig. 15 compatibility studies

The MET and formulation excipient compatibility studies were performed for one month and found no interaction in drug and excipient as characteristic peaks did not change for drug (Fig.15) solid lipids, GMS exhibited slight hydrophilic nature and contributed to increasing the solubility of MET (31). MET displayed the maximum solubility in oleic acid instead of several liquid lipids in this study, whereas Tween 80 demonstrated the highest solubility for MET. The solubility results of MET in the different lipids and surfactants are shown in Table 5 (a), (b) and (c)

Table 5 (a) MET solubility in solid-lipids

Sr. No.	Solid-Lipid	Solubility in mg/g
1	Compritol 888 ATO	4 ± 0.100
2	Precirol ATO 5	6 ± 0.023
3	Glycerol monostearate	17 ± 0.200
4	Cetyl palmitate	7 ± 0.420

Table 5 (b) MET solubility in liquid-lipids

Sr. No.	Liquid-lipids	Solubility in mg/mL
1	Oleic acid	1.69 ± 0.031
2	Capryol 90	1.20 ± 0.024
3	Miglyol 812 N	0.54 ± 0.012

Table 5 (c) MET solubility in surfactants

Sr. No.	Surfactants	Solubility in mg/mL
1	Tween 80	3.6 ± 0.014
2	Kolliphor RH 40	1.5 ± 0.041

Based on the literature, $_{GMS}$MET-NLC formula was successfully optimized using 3^3 BBD (Design-Expert® software) in which the solid-lipid: liquid-lipid (%), surfactant concentration (%) and sonication- time (min) were kept as independent variables while PS, PDI, and EE (%) were kept as the dependent variables. Further, the influence of the interactions of independent variables on PS, PDI, and EE (%) was evaluated through response surface plots as shown in Fig. 16. The Final optimized formula showed 59.66:40.44 % of lipid ratio (120 mg of GMS and 80 mL of oleic acid), 0.69% (138 mg) of surfactant concentration for 20 mL formulation, and 5.11 min as an

ultrasonication time resulted in 114.32 nm (PS), 0.269 (PDI), and 60.1% (% EE), accordingly in Table 3.

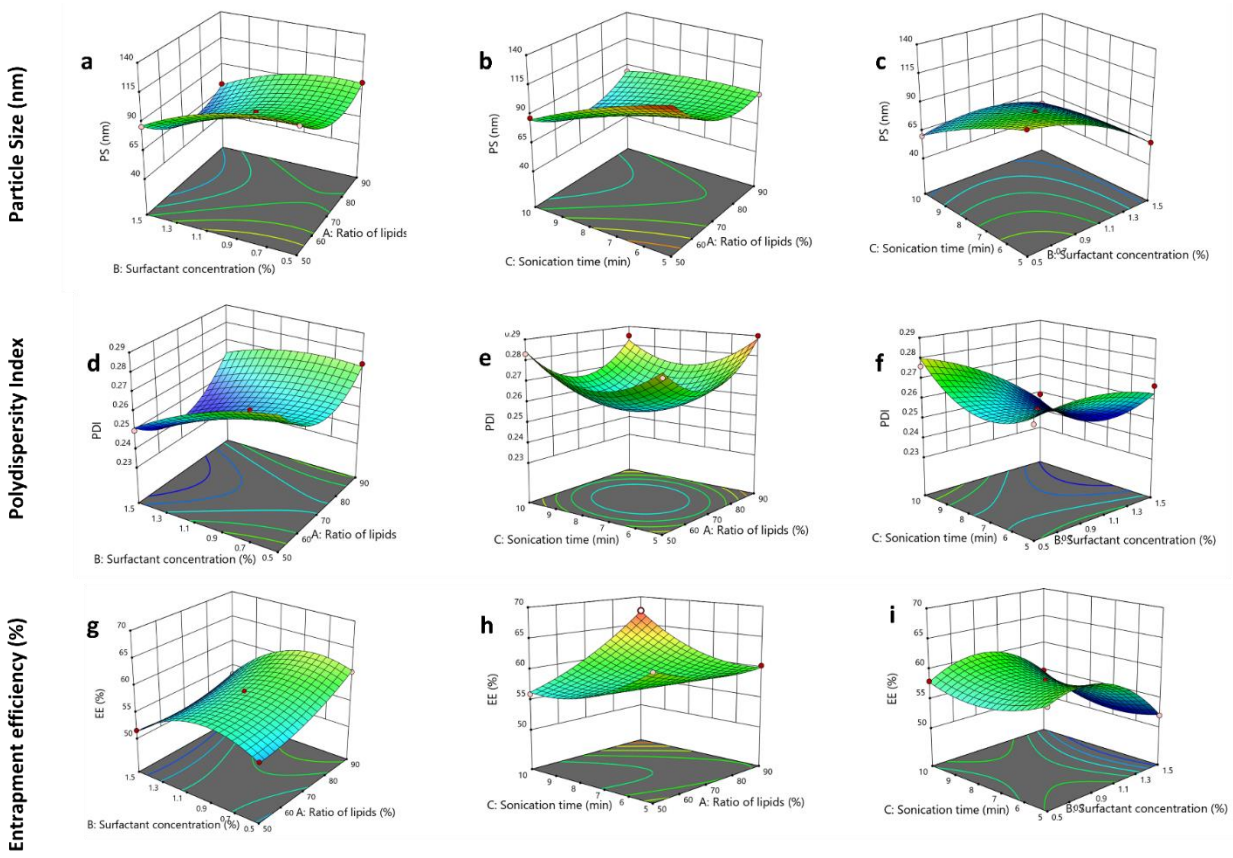

Fig. 16 represents 3-D surface plots shows the interactions of the variables

A $_{GMS}$MET-NLC demonstrated slightly increased PS in comparison to the blank NLC (Table 6),

Table 6. Characterization parameters for plain NLC and optimized formulations

Formulation	PS (nm)	PDI	ZP (mV)	EE (%)	DL (%)
Plain NLC	113.8 ± 0.61	0.276 ± 1.25	-16.00 ± 0.12	--	--
$_{GMS}$MET-NLC	114.9 ± 1.32	0.268 ± 0.04	-15.76 ± 1.34	60.10 ± 2.23	5.5 ± 0.12

PXRD studies showed that (Fig. 17) change of the crystalline form of MET into an amorphous form in the developed NLCs (32). Further, it is confirmed from the DSC studies which demonstrated that endothermic peak in the $_{GMS}$MET-NLC formulation indicated the amorphous form of MET in the developed formulation(Fig. 18) (33). The FTIR studies confirms the presence of MET peaks in FT-IR spectra of $_{GMS}$MET-NLC confirms the incorporation of MET in NLC (Fig. 19). The SEM image reveled that, the particles were spherical in shape without aggregation (Fig. 20) (34, 35).

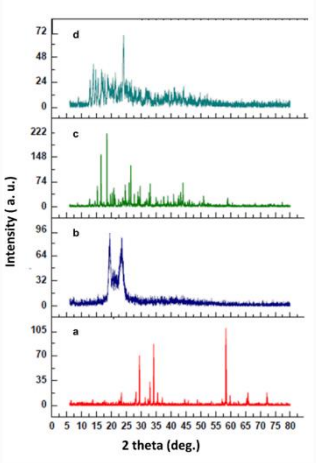

Fig. 17. Diffractograms of MET (a), GMS (b), Trehalose dihydrate (c), and $_{GMS}$MET-NLCs (d)

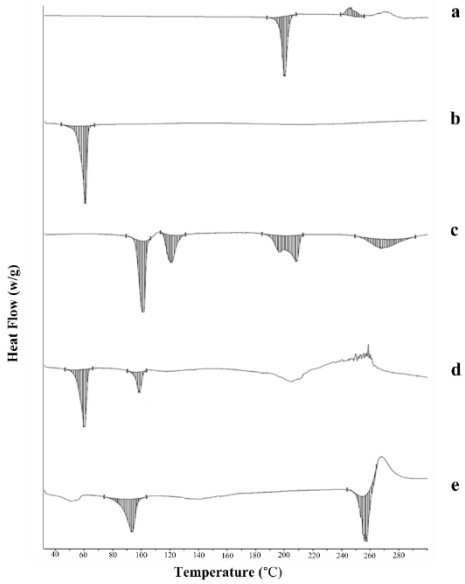

Fig. 18. DSC thermograms of MET (a), GMS (b), Trehalose dihydrate (c), Physical mixture of MET + Excipients (d) and $_{GMS}$MET-NLCs (e)

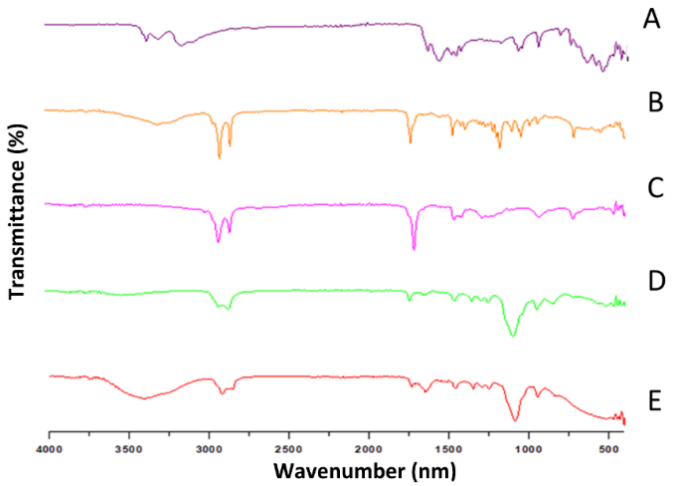

Fig. 19. FTIR spectra of MET (A), GMS (B), Trehalose dihydrate (C), Physical mixture of MET + Excipients (D), and $_{GMS}$MET-NLCs (E)

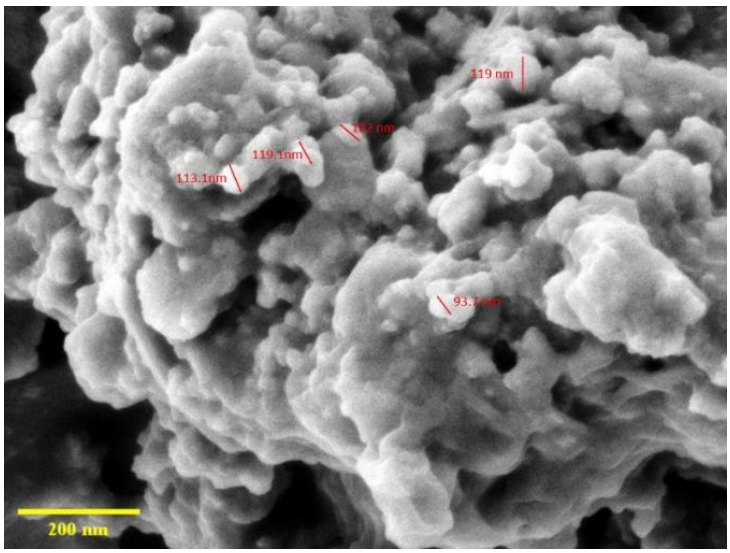

Fig. 20. SEM micrograph image of lyophilized $_{GMS}$MET-NLCs

In-vitro MET release studies shown in Fig. 21 demonstrated that 88 % within 24 h with transport mechanism of MET was to be a Fickian diffusion mechanism as the 'n' value is less than 0.43 (n = 0.38). In the stability studies, a very minute decrease in values of EE and ZP was observed upon storing $_{GMS}$NLC-MET at both conditions. This may be due to the expulsion of the drug oozes out

along with the oleic acid resulting in a decrease in the ZP over the storage period (36). However, the stability study ascertains the physical stability of GMSMET-NLCs

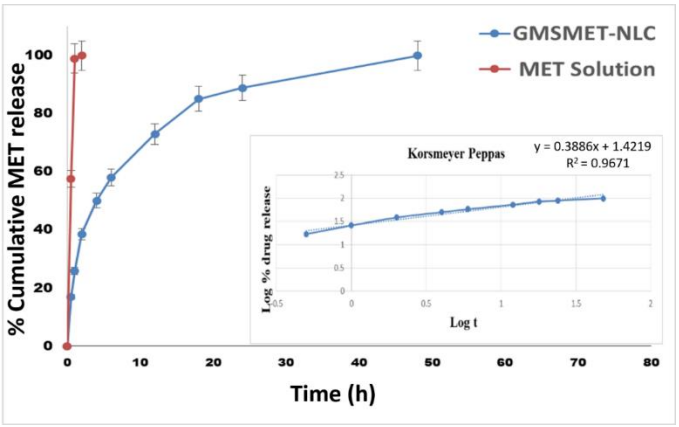

Fig. 21. % Cumulative release profile of MET from GMSMET-NLC in SSF at pH 6.8 and release kinetics (n=3, mean ± SD)

The Cell viability experiment showed in the Fig. 21 that the IC_{50} value for free MET and GMSMET-NLC was 11.40 ± 0.2 mM and 9.54 ± 0.39 mM, respectively after 72 h incubation. Multiple studies reported the budding anticancer activities of MET in a diverse range of cancers. However, the exact mechanism of action is still unclear (37). As per the literature, MET was reported to show anticancer activity by potentiating the AMPK pathway to inhibit the mTOR pathway, resulting in cell death due to apoptosis and cell cycle arrest (38). Furthermore, the 5 mM/L and 10 mM/L concentrations of MET were reported to show anticancer action via the AMPK/mTOR pathway (39). GMSMET-NLCs showed a significant rise in the ROS level in KB cells in a time-dependent manner. These results might be due to submicron PS and anionic ZP of the developed GMSMET-NLCs formulation, more favored by the negative KB as shown in Fig. 23.

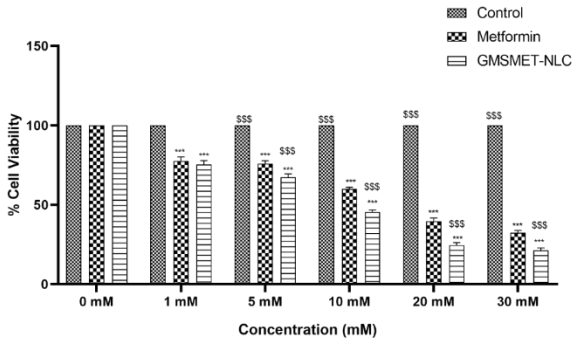

Fig. 22. *In-vitro* cytotoxicity of different concentrations of free MET, MET-NLC to determine IC_{50} value on KB Oral cancer cells after 72 h incubation time.

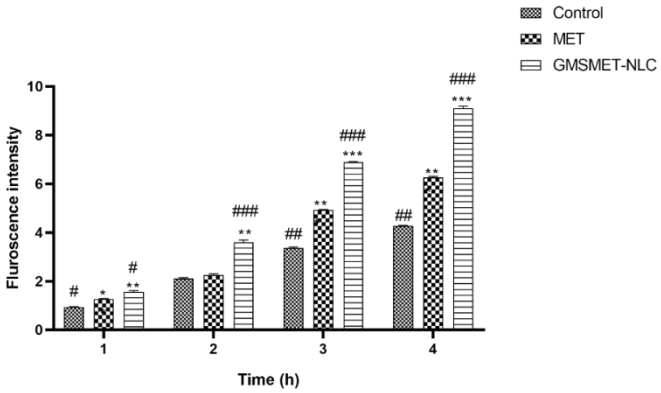

Fig. 23. ROS levels in KB cells after treatment of MET and $_{GMS}$MET-NLC at different time points (n=3, Mean ± SD).

Result & discussion

Part 3: Preparation and *in-vitro* evaluation of lipid nanostructures integrated buccal mucoadhesive thermosensitive gel for dual delivery of silymarin and metformin

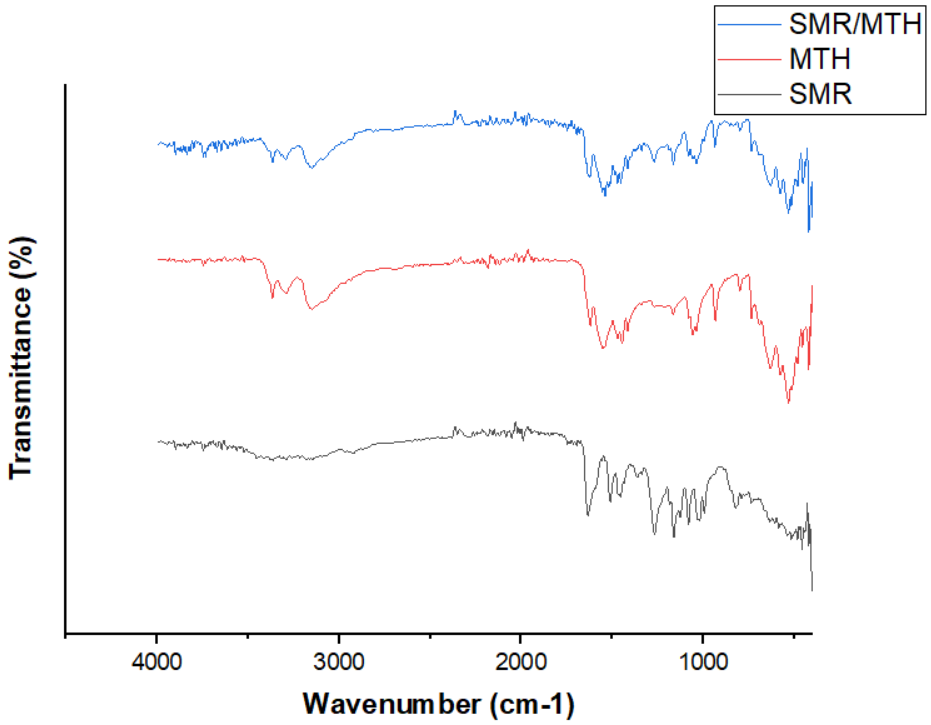

Fig 24. Depicts overlay of Spectra

In the compatibility studies, no significant changes were observed in the characteristic peaks in combination (Fig.24). The trial batches of SME/MET-NLCs were produced with the ratio of solid lipid and liquid lipid at 50:50, 60:40 70:30, 80:20, and, 90:10. We observed, the Compritol ATO 888 and Oleic acid, when mixed at 60: 40 ratios, did not appear as oil droplets on paper. In addition, an appropriate ratio was selected based on PS and % EE of both drugs. The ratio of 60: 40 selected for both lipids with PS 258.9 ± 1.2 nm and % entrapment for MET and SME was 55.2 ± 3.2 % and

67 ± 1.9 % respectively. Besides this, the Kolliphor RH 40 was found to provide the minimum size of the nanoparticle with 0.33 ± 0.5 PDI and -35.6 ± 0.2 mV ZP as shown in **Figure 25.**

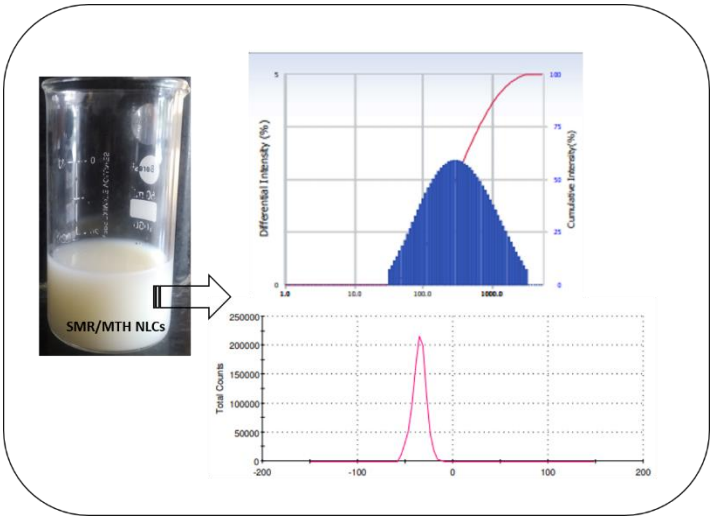

Fig 25. Depicts particle size and zeta potential for SMR/MTH-NLCs

In the surface morphology studies, the SEM and TEM images (Shown in **Fig 26. A and B**) of SMR/MTH NLCs showed the spherical nature of particles. AFM analysis (Fig 27. Demonstrated different parameter for particles shown in Table 7.

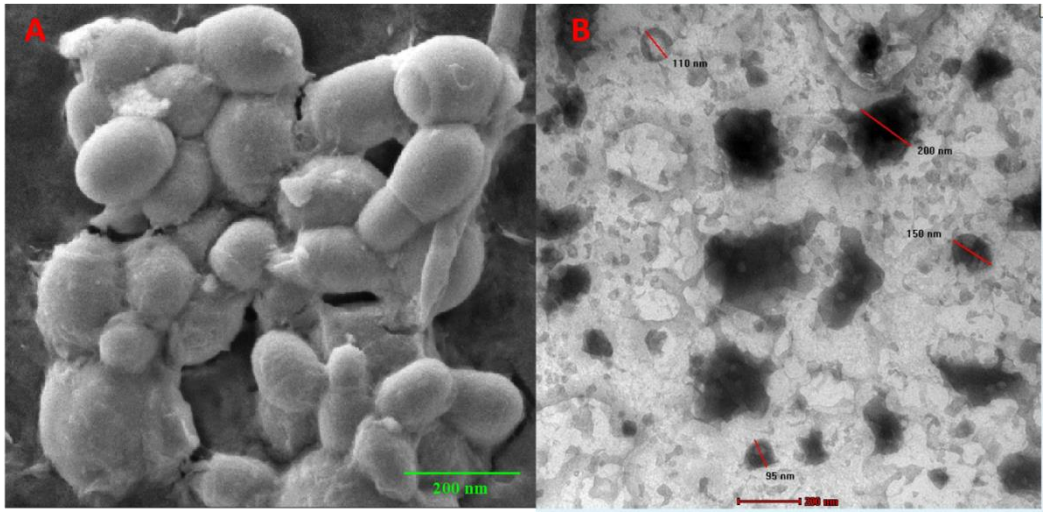

Fig 26. A) Represents the SEM image B) TEM image of SMR/MTH-NLCs

Table 7. Surface properties of SMR/MTH NLCs

S. N.	Surface Characteristics	Measurement
1	Roughness average	10.12 nm
2	Skewness	0.92
3	Kurtosis	5.345

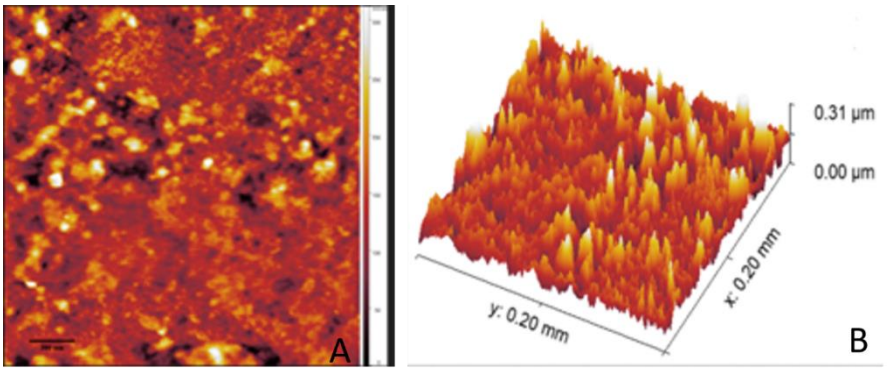

Fig 27. A) Depicts 2D, B) 3D image of SMR/MTH-NLCs Batch

Fig 28 demonstrated about 65% and 55% of MTR and SMR were liberated within 12 h. owing to dissimilar physicochemical properties of MTH and SMR resulting in a difference in the release. To achieve the site-specific application of the formulation, transforming from sol to gel is essential at oral cavity temperature. Therefore, the concentration of P 127 and gellan gum at 0.5 % was selected to show optimum temperature and viscosity with mucoadhesive strength (Fig 29 A) Gelling temperature B) viscosity, and C) mucoadhesive strength of all developed batches). Fig 30. B depicted the gelling of formulation at 35.2 ± 0.5 ℃.

In the *ex-vivo* permeation studies (Fig 31) about 46.10 % MTH and SMR 35.20 % were permeated through goat buccal mucosa form developed gel after 12 h. In the cell viability studies, assess the cytotoxic potential in the combination of SMR and MTH, we treated a combination of free drug, SMR/MTH-NLCs, and mucoadhesive in-situ gel containing SMR/MTH-NLCs in a constant ratio of 1: 250 against KB cells. We obtained the IC_{50} values (Fig 32.) for free SMR/MTH, SMR/MTH-NLCs, and SMR/MTH gel form were 0.89±0.9 µM, 0.72±0.34 µM, and 0.65±1.2 µM, respectively.

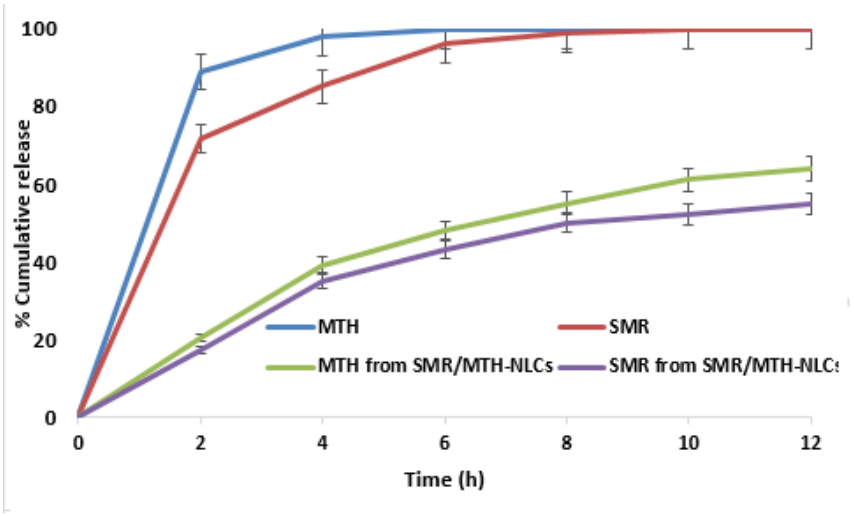

Fig 28. Depicts the release of SMR and MTH from NLCs

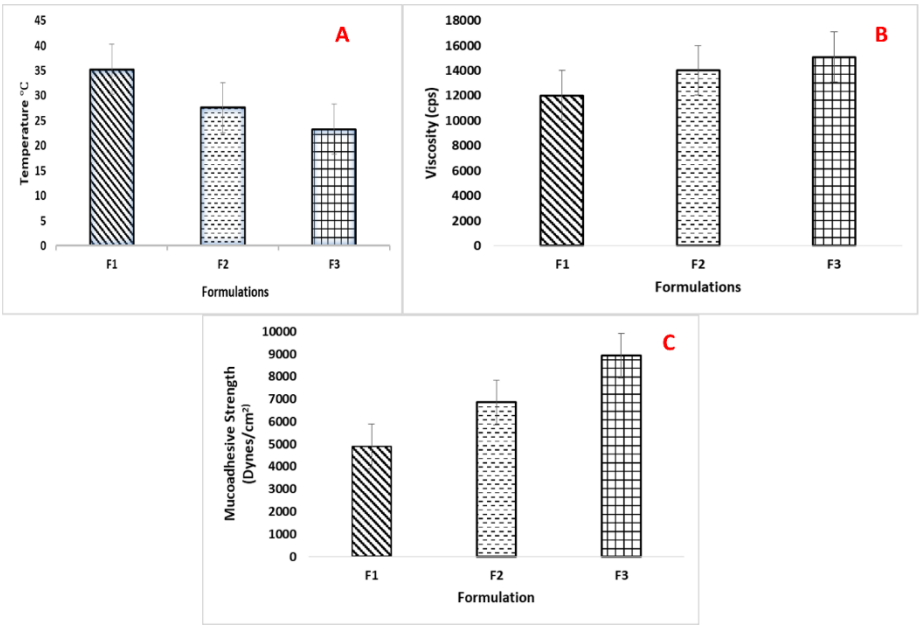

Fig 29. A) Gelling temperature B) viscosity, and C) mucoadhesive strength of all developed batches

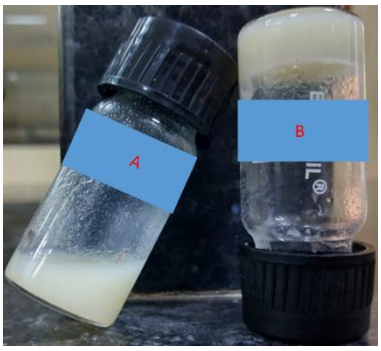

Fig 30. A) Gelling liquid at room temperature and B) gel at 35.2 ± 0.5 ℃

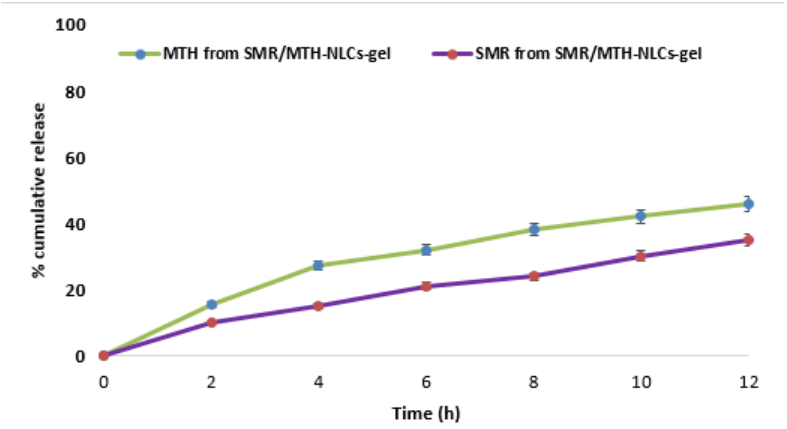

Fig 31. Depicts % cumulative release of SMR and MTH from SMR/MTH-NLC-gel

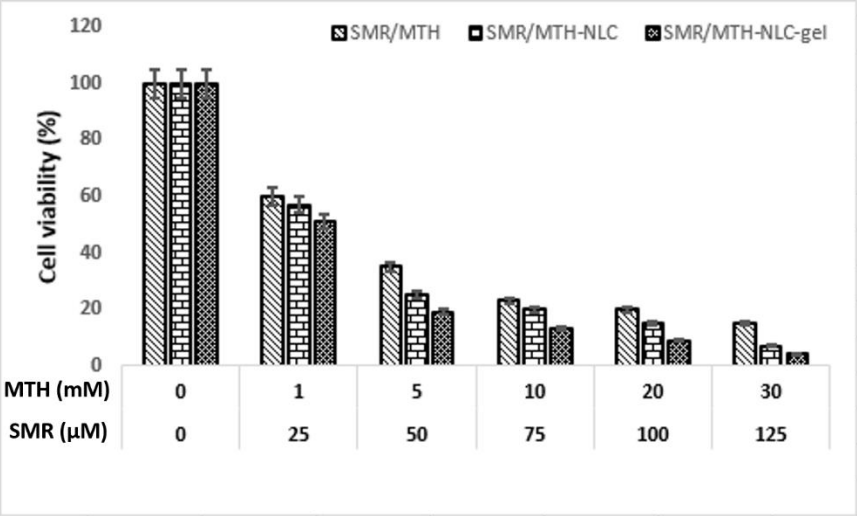

Fig 31. *In-vitro* cell viability of SMR/MTH, SMR/MTH-NLCs, and SMR/MTH-NLC-gel against KB cells treated for 72 h. The values represents the mean of triplicate experiments.

PUBLICATIONS

1) **Shete, M.B**., Deshpande, A.S. and Shende, P., 2022. Silybin-based herbal nanocarriers: an advancement in anticancer therapy. *Materials Technology*, *37*(13), p.2832-2852. **(IF: 3.297)**

2) **Shete, M.B.,** Deshpande, A.S. and Shende, P., 2023. Enhancement of in-vitro anti-oral cancer activities of silymarin using dispersion of nanostructured lipid carrier in mucoadhesive in-situ gel. *International Journal of Pharmaceutics*, *636*, p.122860. **(IF: 6.510)**

3) **Shete, M.B**., Deshpande, A.S. and Shende, P.K., 2023. Nanostructured lipid carrier-loaded metformin hydrochloride: Design, optimization, characterization, assessment of cytotoxicity and ROS evaluation. *Chemistry and Physics of Lipids*, *250*, p.105256. **(IF: 3.570)**

4) Shete M. B., Deshpande A. S. Preparation and *in-vitro* evaluation of lipid nanostructures integrated buccal mucoadhesive thermosensitive gel for dual delivery of silymarin and metformin. Communicated to *Assay and Drug Development Technologies* (IF: 2.471)

CONFERENCES, WORKSHOPS, PRESENTATIONS

1) Successfully completed "Two Days Workshop on QbD & Hands on Training on DoE, at SVKM's, NMIMS, SPTM, Shirpur, Dated – 6^{th} - 7^{th} Oct 2017.

2) Successfully completed "3^{rd} Online International flowcytometry course" organised by Trust for Education and Training in Cytometry (TECT, India), dated 21^{st} to 24 September 2022.

References

1. Dalanon J, Matsuka YJAPJoCPA. Decreased Global Interest in Oral Cancer During the COVID-19 Pandemic. 2021;22(7):2117.

2. Tahmasebi E, Alikhani M, Yazdanian A, Yazdanian M, Tebyanian H, Seifalian A. The current markers of cancer stem cell in oral cancers. Life sciences. 2020;249:117483.

3. Kolokythas A. Long-Term Surgical Complications in the Oral Cancer Patient: a Comprehensive Review. Part II. J Oral Maxillofac Res. 2010;1(3):e2.

4. Thanki K, Gangwal RP, Sangamwar AT, Jain S. Oral delivery of anticancer drugs: challenges and opportunities. Journal of controlled release : official journal of the Controlled Release Society. 2013;170(1):15-40.

5. Landman GW, Kleefstra N, van Hateren KJ, Groenier KH, Gans RO, Bilo HJ. Metformin associated with lower cancer mortality in type 2 diabetes: ZODIAC-16. Diabetes care. 2010;33(2):322-6.

6. Ben Sahra I, Laurent K, Loubat A, Giorgetti-Peraldi S, Colosetti P, Auberger P, et al. The antidiabetic drug metformin exerts an antitumoral effect in vitro and in vivo through a decrease of cyclin D1 level. Oncogene. 2008;27(25):3576-86.

7. Kisfalvi K, Eibl G, Sinnett-Smith J, Rozengurt E. Metformin disrupts crosstalk between G protein-coupled receptor and insulin receptor signaling systems and inhibits pancreatic cancer growth. Cancer research. 2009;69(16):6539-45.

8. Ashinuma H, Takiguchi Y, Kitazono S, Kitazono-Saitoh M, Kitamura A, Chiba T, et al. Antiproliferative action of metformin in human lung cancer cell lines. Oncology reports. 2012;28(1):8-14.

9. Luo Q, Hu D, Hu S, Yan M, Sun Z, Chen F. In vitro and in vivo anti-tumor effect of metformin as a novel therapeutic agent in human oral squamous cell carcinoma. BMC cancer. 2012;12:517.

10. Samadzadeh S, Mousazadeh H, Ghareghomi S, Dadashpour M, Babazadeh M, Zarghami NJJoDDS, et al. In vitro anticancer efficacy of Metformin-loaded PLGA nanofibers towards the post-surgical therapy of lung cancer. 2021;61:102318.

11. Agrawal M, Saraf S, Saraf S, Dubey SK, Puri A, Gupta U, et al. Stimuli-responsive In situ gelling system for nose-to-brain drug delivery. Journal of controlled release : official journal of the Controlled Release Society. 2020;327:235-65.

12. Sood S, Jain K, Gowthamarajan K. Optimization of curcumin nanoemulsion for intranasal delivery using design of experiment and its toxicity assessment. Colloids and Surfaces B: Biointerfaces. 2014;113:330-7.
13. Zhang W, Li X, Ye T, Chen F, Sun X, Kong J, et al. Design, characterization, and in vitro cellular inhibition and uptake of optimized genistein-loaded NLC for the prevention of posterior capsular opacification using response surface methodology. International journal of pharmaceutics. 2013;454(1):354-66.
14. Singh H, Sharma R, Joshi M, Garg T, Goyal AK, Rath G. Transmucosal delivery of Docetaxel by mucoadhesive polymeric nanofibers. Artificial cells, nanomedicine, and biotechnology. 2015;43(4):263-9.
15. Gade S, Patel KK, Gupta C, Anjum MM, Deepika D, Agrawal AK, et al. An Ex Vivo Evaluation of Moxifloxacin Nanostructured Lipid Carrier Enriched In Situ Gel for Transcorneal Permeation on Goat Cornea. Journal of pharmaceutical sciences. 2019;108(9):2905-16.
16. Schmolka IR. Artificial skin I. Preparation and properties of pluronic F-127 gels for treatment of burns. Journal of biomedical materials research. 1972;6(6):571-82.
17. Pagano C, Giovagnoli S, Perioli L, Tiralti MC, Ricci MJEJoPS. Development and characterization of mucoadhesive-thermoresponsive gels for the treatment of oral mucosa diseases. 2020;142:105125.
18. Yu S, Tan G, Liu D, Yang X, Pan WJRa. Nanostructured lipid carrier (NLC)-based novel hydrogels as potential carriers for nepafenac applied after cataract surgery for the treatment of inflammation: design, characterization and in vitro cellular inhibition and uptake studies. 2017;7(27):16668-77.
19. Lu S, Yu P-p, He J-H, Zhang S-s, Xia Y-L, Zhang W-L, et al. Enhanced dissolution and oral bioavailability of lurasidone hydrochloride nanosuspensions prepared by antisolvent precipitation–ultrasonication method. RSC advances. 2016;6(54):49052-9.
20. Natarajan J, Baskaran M, Humtsoe LC, Vadivelan R, Justin A. Enhanced brain targeting efficacy of Olanzapine through solid lipid nanoparticles. Artificial cells, nanomedicine, and biotechnology. 2017;45(2):364-71.
21. Nasra MM, Khiri HM, Hazzah HA, Abdallah OY. Formulation, in-vitro characterization and clinical evaluation of curcumin in-situ gel for treatment of periodontitis. Drug delivery. 2017;24(1):133-42.

22. Kesharwani P, Jain A, Srivastava AK, Keshari MK. Systematic development and characterization of curcumin-loaded nanogel for topical application. Drug development and industrial pharmacy. 2020;46(9):1443-57.
23. Mura P, Mennini N, Nativi C, Richichi B. In situ mucoadhesive-thermosensitive liposomal gel as a novel vehicle for nasal extended delivery of opiorphin. European Journal of Pharmaceutics and Biopharmaceutics. 2018;122:54-61.
24. Pandit AP, Pol VV, Kulkarni VS. Xyloglucan Based In Situ Gel of Lidocaine HCl for the Treatment of Periodontosis. Journal of pharmaceutics. 2016;2016:3054321.
25. Ajiboye AL, Nandi U, Galli M, Trivedi V. Olanzapine Loaded Nanostructured Lipid Carriers via High Shear Homogenization and Ultrasonication. Scientia Pharmaceutica. 2021;89(2):25.
26. Kaithwas V, Dora CP, Kushwah V, Jain S. Nanostructured lipid carriers of olmesartan medoxomil with enhanced oral bioavailability. Colloids and Surfaces B: Biointerfaces. 2017;154:10-20.
27. Krambeck K, Silva V, Silva R, Fernandes C, Cagide F, Borges F, et al. Design and characterization of Nanostructured lipid carriers (NLC) and Nanostructured lipid carrier-based hydrogels containing Passiflora edulis seeds oil. 2021;600:120444.
28. Garala K, Joshi P, Shah M, Ramkishan A, Patel J. Formulation and evaluation of periodontal in situ gel. International journal of pharmaceutical investigation. 2013;3(1):29.
29. Hosny KM, Rizg WY, Khallaf RA. Preparation and Optimization of In Situ Gel Loaded with Rosuvastatin-Ellagic Acid Nanotransfersomes to Enhance the Anti-Proliferative Activity. Pharmaceutics. 2020;12(3).
30. Ramakrishnan G, Lo Muzio L, Elinos-Báez CM, Jagan S, Augustine TA, Kamaraj S, et al. Silymarin inhibited proliferation and induced apoptosis in hepatic cancer cells. Cell Prolif. 2009;42(2):229-40.
31. Ghasemian E, Vatanara A, Navidi N, Rouini MR. Brain delivery of baclofen as a hydrophilic drug by nanolipid carriers: Characteristics and pharmacokinetics evaluation. Journal of Drug Delivery Science and Technology. 2017;37:67-73.
32. Ebrahimi S, Farhadian N, Karimi M, Ebrahimi M. Enhanced bactericidal effect of ceftriaxone drug encapsulated in nanostructured lipid carrier against gram-negative Escherichia

coli bacteria: drug formulation, optimization, and cell culture study. Antimicrobial Resistance & Infection Control. 2020;9(1):1-12.

33. Deshkar SS, Jadhav MS, Shirolkar SV. Development of Carbamazepine Nanostructured Lipid Carrier Loaded Thermosensitive Gel for Intranasal Delivery. Advanced Pharmaceutical Bulletin. 2021;11(1):150.

34. Dubes A, Parrot-Lopez H, Abdelwahed W, Degobert G, Fessi H, Shahgaldian P, et al. Scanning electron microscopy and atomic force microscopy imaging of solid lipid nanoparticles derived from amphiphilic cyclodextrins. European journal of pharmaceutics and biopharmaceutics : official journal of Arbeitsgemeinschaft fur Pharmazeutische Verfahrenstechnik eV. 2003;55(3):279-82.

35. Almalik A, Alradwan I, Kalam MA, Alshamsan A. Effect of cryoprotection on particle size stability and preservation of chitosan nanoparticles with and without hyaluronate or alginate coating. Saudi pharmaceutical journal : SPJ : the official publication of the Saudi Pharmaceutical Society. 2017;25(6):861-7.

36. Murthy A, Rao Ravi P, Kathuria H, Malekar SJN. Oral bioavailability enhancement of raloxifene with nanostructured lipid carriers. 2020;10(6):1085.

37. Tan BX, Yao WX, Ge J, Peng XC, Du XB, Zhang R, et al. Prognostic influence of metformin as first-line chemotherapy for advanced nonsmall cell lung cancer in patients with type 2 diabetes. 2011;117(22):5103-11.

38. Shen M, Zhang Z, Ratnam M, Dou QPJJocp. The interplay of AMP-activated protein kinase and androgen receptor in prostate cancer cells. 2014;229(6):688-95.

39. Martin-Castillo B, Vazquez-Martin A, Oliveras-Ferraros C, Menendez JAJCc. Metformin and cancer: doses, mechanisms and the dandelion and hormetic phenomena. 2010;9(6):1057-64.

Meghanath B. Shete
Research Scholar

Supervisor

Dr. Ashwini S. Deshpande
Professor & Associate Dean
NMIMS, SPTM
Hyderabad Campus